METHODOLOGY

An optimized protocol for the generation and monitoring of conditional orthotopic lung cancer in the KP mouse model using an adeno-associated virus vector compatible with biosafety level 1

Haibin Deng[1,2,9,10] · Huixiang Ge[1,2,3] · Christelle Dubey[1,2] · Tereza Losmanova[4] · Michaela Medová[2,5] ·
Georgia Konstantinidou[6] · Seyran Mathilde Mutlu[2,7] · Fabienne Esther Birrer[8,2] · Tess Melinda Brodie[8,2] ·
Deborah Stroka[8,2] · Wenxiang Wang[9,10] · Ren-Wang Peng[1,2] · Patrick Dorn[1,2] · Thomas Michael Marti[1,2]

Abstract

Background The inducible Kras/p53 lung adenocarcinoma mouse model, which faithfully recapitulates human disease, is routinely initiated by the intratracheal instillation of a virus-based Cre recombinase delivery system. Handling virus-based delivery systems requires elevated biosafety levels, e.g., biosafety level 2 (BSL-2). However, in experimental animal research facilities, following exposure to viral vectors in a BSL-2 environment, rodents may not be reclassified to BSL-1 according to standard practice, preventing access to small animal micro-computed tomography (micro-CT) scanners that are typically housed in general access areas such as BSL-1 rooms. Therefore, our goal was to adapt the protocol so that the Cre-induced KP mouse model could be handled under BSL-1 conditions during the entire procedure.
Results The Kras-Lox-STOP-Lox-G12D/p53 flox/flox (KP)-based lung adenocarcinoma mouse model was activated by intratracheal instillation of either an adenoviral-based or a gutless, adeno-associated viral-based Cre delivery system. Tumor growth was monitored over time by micro-CT. We have successfully substituted the virus-based Cre delivery system with a commercially available, gutless, adeno-associated, Cre-expressing vector that allows the KP mouse model to be handled and imaged in a BSL-1 facility. By optimizing the anesthesia protocol and switching to a microscope-guided vector instillation procedure, productivity was increased and procedure-related complications were significantly reduced. In addition, repeated micro-CT analysis of individual animals allowed us to monitor tumor growth longitudinally, dramatically reducing the number of animals required per experiment. Finally, we documented the evolution of tumor volume for different doses, which revealed that individual tumor nodules induced by low-titer AAV-Cre transductions can be monitored over time by micro-CT.
Conclusion Modifications to the anesthesia and instillation protocols increased the productivity of the original KP protocol. In addition, the switch to a gutless, adeno-associated, Cre-expressing vector allowed longitudinal monitoring of tumor growth under BSL-1 conditions, significantly reducing the number of animals required for an experiment, in line with the 3R principles.

Keywords Lung adenocarcinoma · Mouse model · BSL-1 · Intratracheal instillation · AAV vector · Cre-expressing vector

Abbreviations

BSL-2	Biosafety level 2
H&E	Hematoxylin & Eosin
KP	Kras-Lox-STOP-Lox-G12D/p53 flox/flox
micro-CT	Micro-computed tomography
NSCLC	Non-small cell lung cancer
PFU	Plaque forming units

Extended author information available on the last page of the article

Background

The broad applicability of the KP model

Orthotopic, genetically engineered mouse models of cancer provide the basis to study tumor initiation, progression, and treatment options in the pathophysiologically relevant tumor microenvironment [27]. Lung cancer is the leading cause of cancer-related deaths worldwide, with more than 80% of lung tumors being non-small cell lung cancer (NSCLC). Oncogenic *KRAS* mutations are frequent in lung and other solid tumors, with a prevalence of approximately 30% in

NSCLC adenocarcinomas [22]. Co-occurring genomic alterations significantly affect the cellular phenotype, clinical outcomes, and therapeutic vulnerabilities of KRAS-mutant cancers. 38% of the human KRAS-mutant lung adenocarcinoma feature an additional loss-of-function mutation in the tumor suppressor *TRP53* [49], which has an overall prevalence of 50–70% in human NSCLC [22].

The first protocol describing the use of a recombinant adenovirus expressing Cre recombinase (adeno-Cre) to induce K-ras G12D expression in mouse lungs was published in 2001 [25], followed by a study in 2005 describing adeno-Cre-mediated activation of K-ras G12D in combination with deletion of p53 [24]. In 2009, Tyler Jacks' group published their step-by-step protocol describing their lung cancer KP model [12], which has since been cited over 500 times.

The proof-of-principle experiments in the initial description were based on the intranasal or intratracheal application of both adeno- and lentivirus-based Cre-recombinase to the lung, resulting in the generation of NSCLC [12]. Consequently, the KP model was mainly used to model NSCLC but also to study tumor formation in other organs, e.g., soft tissue sarcomas [14, 29] and pancreatic ductal adenocarcinomas [35]. More recently, normal colon organoids generated from KP mice were transduced with adenoviral Cre, resulting in the generation of colorectal cancer organoids [46]. This indicates that tumor models from different entities could be generated by the in vitro transformation of normal cells derived from KP animals. To allow for autochthonous tumor initiation, the K and P alleles can be combined with an inducible transgenic allele, in which a tissue-specific or inducible promoter regulates Cre-expression, or the combination thereof, as recently reviewed elsewhere [28]. Alternatively, autochthonous tumors can also be initiated spatiotemporally controlled by delivery of the Cre recombinase by viral vectors, e.g., the initial KP lung adenocarcinoma model [12].

The virus-based delivery of Cre-recombinase typically requires a BSL-2 facility

In the initial study by the Jacks group, both adeno- and lentivirus-based systems were used to deliver Cre recombinase [12]. Due to their potential to enter human cells, deliver genetic material, and elicit an immune response, viral vectors, even when replication-deficient, are typically categorized as a potential biohazard and thus have to be handled at facilities with heightened biosafety measures, i.e., a biosafety level 2 (BSL-2) status. Thus, BSL-2 practices are generally recommended during viral vector administration as it is also recommended by the Viral Vector Core of the University of Iowa (https://vector-core.medicine.uiowa.edu/), e.g., the producer of the adenoviral vector used by

the Jacks group in their initial publication [12]. Further, of 44 institutions using viral vectors in animal research, 66% required that animals receiving lentiviral and adenoviral vectors be housed under BLS-2 conditions for several days after administration or the duration of the experiment [10]. Some facilities allow a reclassification to BSL-1 housing after an initial 72 h period of BSL-2 containment [10]. However, in most animal research facilities, animals previously housed in a BSL-2 facility cannot be reclassified to BSL-1 housing because of the significant additional risk that the animals may have been cross-contaminated in a BSL-2 facility. Problematically, a BSL-2 status might restrict access to the equipment required for the noninvasive analysis of tumor growth over time, i.e., micro-computed tomography (micro-CT). In detail, the equipment to perform micro-CT is expensive. Thus, shared animal facilities seek to maximize unrestricted access and house this type of equipment in rooms with BSL-1 status. To address this issue, we sought to replace the virus-based vectors required for Cre recombinase administration with a vector that can be handled in BSL-1 facilities, a gutless, adeno-associated virus (AAV) vector.

A gutless, adeno-associated virus (AAV) vector for delivery of Cre-recombinase under BSL-1 conditions

Compared to adeno- or lentiviral-based vectors (see also https://www.takarabio.com/learning-centers/gene-function/viral-transduction/recombinant-virus-comparison), vectors based on adeno-associated virus (AAV) feature two main advantages, e.g., decreased immunogenicity and BSL requirements. In detail, adeno- and lentivirus-based vectors trigger a robust humoral and cellular immune response in mice [3, 4]. Anti-AAV humoral responses have also been reported in small animal models. However, although the onset of anti-capsid cellular responses has been observed in several clinical trials, this has never been observed in any of the tested preclinical animal models, even in those susceptible to natural AAV infection, possibly due to difference in the T cell compartment when compared to humans [43].

In the context of biosafety measures, AAV vectors have emerged as one of the most widely used vectors for in vivo gene therapy, e.g., AAV1-based gene therapy for the treatment of lipoprotein lipase deficiency was approved as the first viral vector-based therapy in Europe back in 2012 [41]. The latest generation of recombinant vectors derived from wild-type AAVs and used for gene delivery contains the so-called "gutless" AAV vectors that do not harbor any adenoviral genomic material except for the AAV inverted terminal repeats (ITRS), which serve as a "packaging signal" [45]. According to the NIH guidelines, AAV vectors are classified under risk group 1 (not associated with disease in healthy human adults), given that they do not encode a

toxic or potentially harmful transgene, and that appropriate precautions were taken during vector preparation and administration [10].

Longitudinal monitoring of tumor growth by micro-CT

The original publication of the establishment of the KP tumor model was closely followed by studies showing the feasibility of monitoring this model's tumor formation and growth over time by micro-CT [19] and its tumor response to radiation therapy [30]. Indeed, it was shown that repetitive measurements by micro-CT were not affecting tumor growth over time [17]. Longitudinal monitoring of tumor growth in individual animals of a single animal cohort has several advantages over the analysis of multiple independent cohorts at specific time points. In the first scenario, individual animals can be monitored over time, allowing pairwise statistical analysis of tumor growth. This significantly reduces the number of animals required per experiment and thus has ethical and economic advantages.

In summary, in this report, we present a protocol for adapting the existing KP lung cancer mouse model in which the lentiviral vector is substituted with a gutless AAV vector that allows animals to be handled in a BSL-1 facility. The BSL1 status of the animals allows repeated monitoring of tumor growth over time with a micro-CT device, which is rarely available in BSL2 rooms of animal research facilities. In addition, we optimized the anesthetic protocol and switched to a microscope-guided procedure for vector instillation. This has increased efficiency and significantly reduced complications associated with the process, contributing to compliance with the 3Rs principles.

Results

Optimizing the anesthesia protocol and switching to microscope-guided viral instillation increases productivity and reduces procedure-related complications

To adapt the original KP protocol [12] to our setting, we implemented two major changes to the protocol. First, we changed the anesthesia protocol to replace tribromoethanol (trade name Avertin®), which is no longer manufactured as a pharmaceutical-grade drug and is also listed as an inadmissible anesthetic in Switzerland (https://www.blv.admin.ch/blv/en/home/suche.html#Tribromoethanol). We first switched to Ketamine/Xylazine-based anesthesia, which was previously regarded as the agent

of choice for rodent injectable anesthesia [8]. However, in our hands, this resulted in unstable anesthesia, which made the subsequent intratracheal instillation very difficult. In addition, this protocol resulted in long recovery times as reported before [2], and also animal death. Subsequently, we switched to a Ketalar, Domitor, and Fentanyl-based anesthetic protocol [1]. The Ketalar and Fentanyl-based anesthetic protocol resulted in the rapid onset of deep anesthesia. In addition, the availability of an antidote in the protocol significantly shortened the follow-up time. As a second measure, we began to perform intratracheal instillation using a stereomicroscope (Fig. 1). This allowed us to easily distinguish the trachea illuminated by the flashlight from the esophagus. The adapted anesthetic protocol combined with the microscopy-based inoculation protocol increased our productivity, e.g., routinely instilling 10–12 animals per hour. In addition, we have performed approximately 100 procedures with our adapted protocol to date, but only three animals have died. Thus, in our hands, the two modifications significantly increased productivity and reduced the rate of procedure-related deaths.

Tumor initiation by a gutless AAV-Cre vector does not alter disease onset or stage in comparison with the AV-based KPL model

We aimed to optimize the KP model without changing its phenotype. In the initial publication, the Jack's group monitored tumor development and progression based on the analysis of histological sections [12]. The KP model results in a multi-focal disease in which individual tumors are not at the same stage of disease development. Thus, the initial study employed a four-stage grading system for tumor progression. 10 weeks after the application of an adeno-Cre virus at a dose of 2.5×10^7 plaque forming units (PFU), we also observed tumors of all four grades, which were detectable after H&E staining of histological sections (Fig. 2A). While a functional titer was determined for the adeno-Cre virus, i.e., the titer was expressed in PFU, a physical titer was determined for the AAV-Cre vector, i.e., viral genomes (VG). It was found that the conversion of PFU to VG was highly variable, e.g., the ratio varied from 1:10 to 1:3600 for the conversion of physical units to biological activity [18]. Therefore, we assumed that the actual biological activity would be 100-fold lower when the titer was determined as VG compared to PFU. Indeed, 12 weeks after the application of the AAV-Cre vector at a dose of 2.5×10^9 viral genomes (VG), a similar tumor burden was observed (analysis after 10 weeks was performed by micro-CT, see Fig. S1). Further, all four stages of tumor progression were detectable in histological H&E sections independently of the virus titer (Fig. 2B).
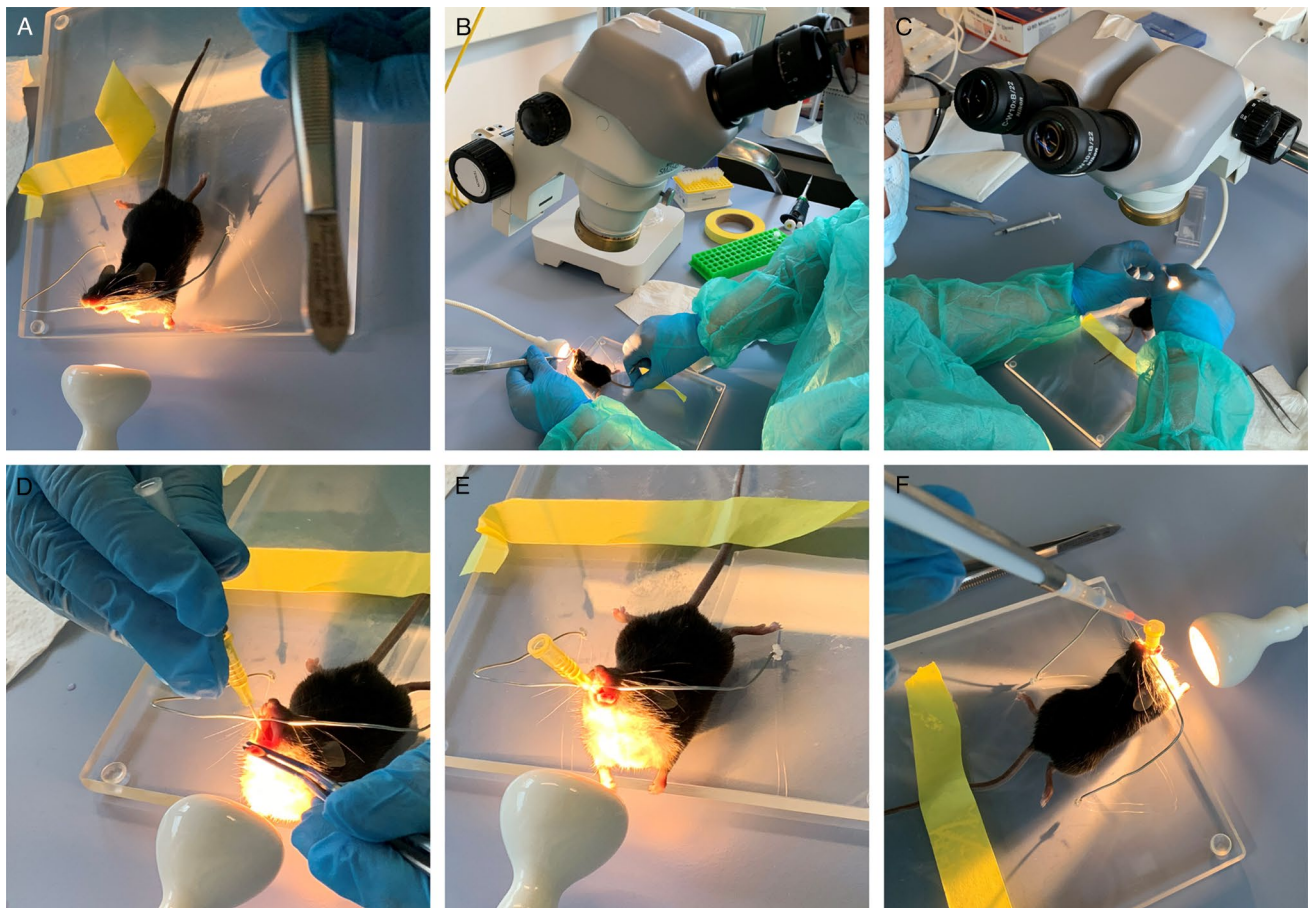
Fig. 1 Microscope-guided viral instillation increases productivity and reduces procedure-related complications. Depiction of the procedure for administering infectious solutions by intratracheal instillation based on the original KP protocol by DuPage et al. [12]. As a modification, a stereomicroscope is used to guide the insertion of the cannula and the subsequent steps of inoculation with the infectious solution. The procedure is described in detail under "Administration of viruses/vectors by intratracheal instillation" in the Materials and Methods section

The adaptation of the virus titer can control the degree of tumor burden

We titrated the AAV-Cre virus stock to mimic the adeno-Cre-induced tumor development. Indeed, instillation with increasing doses of AAV-Cre virus resulted in increased tumor burden (Fig. 2A). Further, this was also accompanied by an increase in the area with tumor-associated inflammation, e.g., regions of lung tissue with increased H&E staining (Fig. 2A, 0.5×10^9 VG, lung parenchyma of the left compared to the right lower lobe, respectively). In summary, based on the analysis of the histology sections, substituting the adeno-Cre with an AAV-Cre virus resulted in a similar onset and tumor stage pattern of the disease as observed in the original KP model.

Longitudinal monitoring of KP tumor growth by micro-CT

The KP model has already been combined with the analysis by micro-CT for longitudinal monitoring of tumor growth per se or after additional radiotherapy [19, 30]. Due to the reduced biosafety requirements of the AAV-Cre vector, we were able to move the animals between the animal holding area and the room where the micro-CT unit was located, both of which were in the BSL-1 zone of our animal facility. This allowed us to monitor tumor growth over time using sequential micro-CT. The analysis by micro-CT revealed that 4 weeks after inoculation with different virus doses, no individual tumor nodules were detectable (Fig. 3). 6 weeks after inoculation with a high virus dose, e.g., 2.5

and 12.5×10^9 VG, respectively, few single nodules became evident. Others showed that 8 weeks after infection of KP animals with a high dose of adeno-Cre virus, regions with a high signal intensity were detectable by micro-CT, and those regions were associated with increased macrophage infiltration [19]. Indeed, large areas with increased signal intensity became noticeable after infection of KP animals with a high dose of adeno-Cre virus (Fig. 3A, 6 weeks, 2.5 and 12.5×10^9 VG).

Early onset disease with a heavy tumor burden induced by high-titer AAV-Cre vector transduction can be monitored by 3D reconstruction

Due to the multiplicity and complexity of tumor formation induced by a high titer virus infection, identifying and quantifying individual tumor nodules over time is not feasible. Therefore, Haines et al. developed an analytical method to quantitatively measure total lung tumor burden based on micro-CT imaging [19]. In detail, tumor tissue cannot readily be distinguished from vasculature by non-contrast micro-CT since the two tissues have similar X-ray densities [19]. However, the total tumor burden correlates proportionally with the combined tumor and vasculature volume in the lung, which, when subtracted from the total chest space, can be used to calculate the remaining functional lung volume as recently described by us before [11]. Indeed, 8 weeks after inoculation with high virus doses, e.g., 2.5 and 12.5×10^9 VG, respectively, tumor lesions became visually detectable in the 3D reconstruction of the intact lung volume (Fig. 3A, 6 weeks, 2.5 and 12.5×10^9 VG). In the 3D reconstructions, lesions increased visually over time, e.g., at 8 and 12 weeks after inoculation with higher viral doses. After the inoculation with 2.5 and 12.5×10^9 VG, the mean functional lung volume was significantly reduced compared with the group inoculated with a low dose of 0.1×10^9 VG (Fig. 3A, right side, bottom left and bottom right panels, respectively, and Fig. 3B). Interestingly, although significant changes in normal lung volume were detectable over time, this did not yet translate in reduced body weight during the observation period (Fig. 3B).

Single tumor nodules induced by low-titer AAV-Cre vector transductions can be monitored over time by micro-CT

In humans, lung cancer usually appears as a single tumor nodule at the time of diagnosis. Previously, a single KP tumor nodule was induced by intrathoracic injection of the adeno-Cre virus to recapitulate human disease and serve as a preclinical model for testing treatments for localized disease, e.g., radiotherapy [23]. We observed that after a prolonged latency period following inoculation with a low viral titer,

e.g., 0.1×10^9 and 0.5×10^9 VG, respectively, few lesions appeared, and individual nodules became readily detectable by micro-CT (Fig. 3C, D).

Finally, analysis of formalin-fixed, paraffin-embedded samples by imaging mass cytometry revealed that individual tumor nodules formed after inoculation with a low viral titer of 0.1×10^9 VG were readily distinguishable by the accumulation of increased E-cadherin signal intensity (Fig. 4). A significant proportion of the nodules did not show increased infiltration with immune cells compared with surrounding lung tissue (Fig. 4A). This is in agreement with previous publications, which indicated that the lack of neoantigens in the KP model results not elicit tumor-specific T cell responses [12, 16]. However, a subset of tumor nodules exhibited significant infiltration by CD8-positive cells, a critical subpopulation of MHC class I-restricted T cells that are mediators of adaptive immunity (Fig. 4B). Infiltration with CD8-positive cells was often accompanied by infiltration of the immediate nodal environment by CD206-positive cells (Fig. S2), e.g., a marker of activated tumor-associated macrophages associated with enhancement of the adaptive and innate antitumor immune responses [26]. Because the AAV vector used in our study does not lead to the expression of neoantigens associated with lentiviral vector integration [13], it will be interesting to investigate what drives the observed inflammation in a subset of tumor nodules induced by AAV-Cre transduction in the KP lung cancer model.

Discussion

In this study, we implemented several changes to the original KP tumor model. Regarding the biosafety aspects of our protocol adaptations: the latest generation of "gutless" AAV vectors contains no adenoviral genomic material except for the adenoviral packaging signal. They are thus entirely replication-deficient and cannot be restored by recombination events, which pose a biohazard thread during the production of lentiviral particles. Thus, AAV particles, in the absence of a toxic or hazardous transgene, can be handled at BSL-1 facilities. Cre-recombinase is not considered a biohazard, according to NIH guidelines. In addition, the Cre-expressing AAV used in our study is commercially available (EPFL's PTBTG gene therapy platform (https://www.epfl.ch/research/facilities/gene-therapy/), which facilitates the transition to the adapted protocol for other research groups.

In our current version of the protocol, $CaCl_2$ is added to a final concentration of 10 mM because it has been shown that incorporation of AAV into a calcium-phosphate coprecipitate enhances gene transfer to airway epithelia in vitro and in vivo [44]. However, a recent publication indicated that the addition of $CaCl_2$ could actually inhibit the transduction efficiency of AAV2 vectors, whereas the combined use of
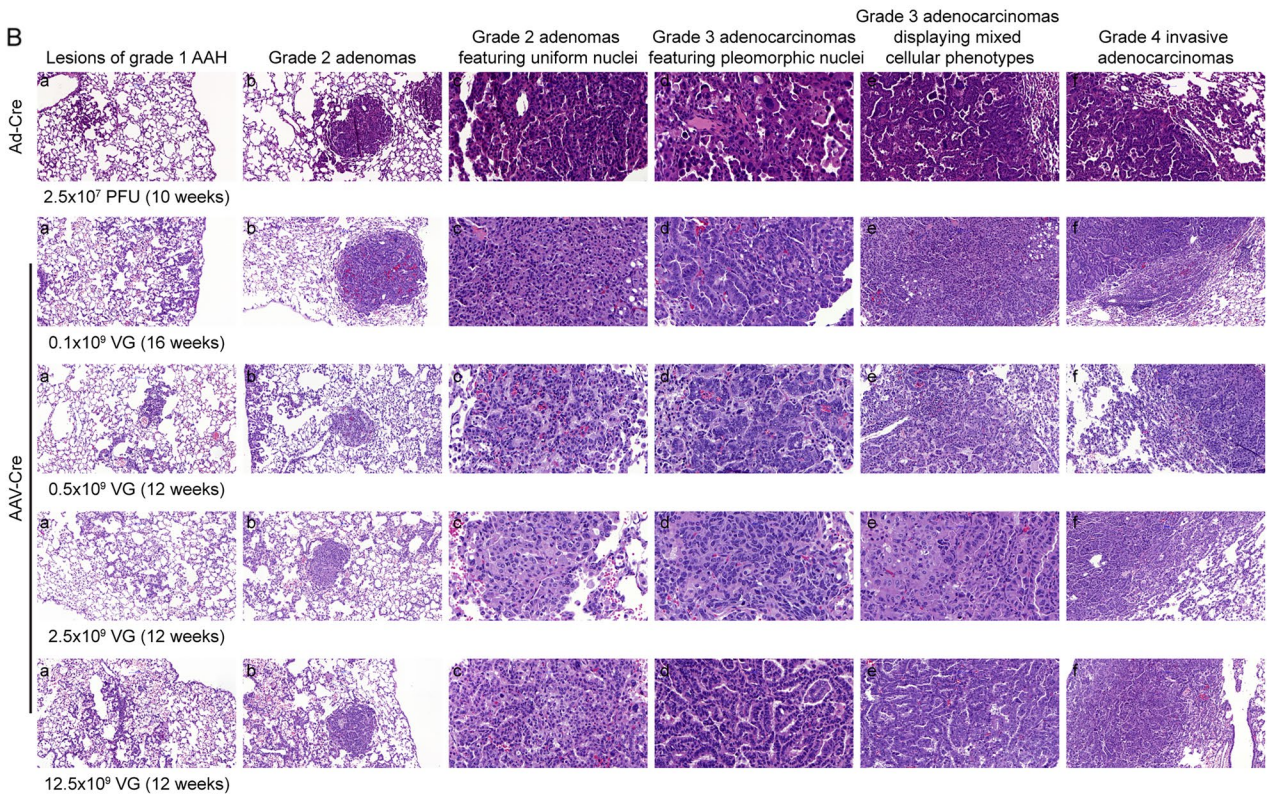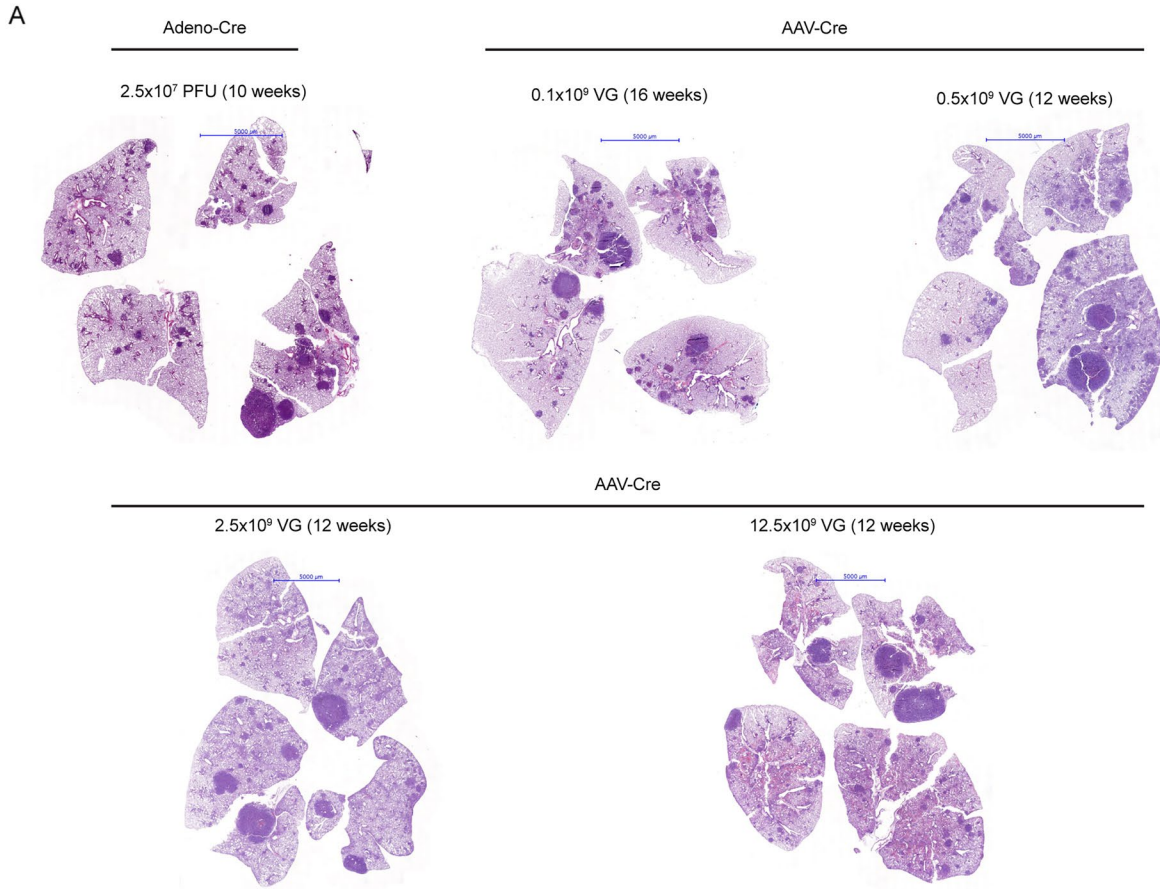
A

Adeno-Cre

2.5x10^7 PFU (10 weeks)

AAV-Cre

0.1x10^9 VG (16 weeks)

0.5x10^9 VG (12 weeks)

AAV-Cre

2.5x10^9 VG (12 weeks)

12.5x10^9 VG (12 weeks)

B

| | Lesions of grade 1 AAH | Grade 2 adenomas | Grade 2 adenomas featuring uniform nuclei | Grade 3 adenocarcinomas featuring pleomorphic nuclei | Grade 3 adenocarcinomas displaying mixed cellular phenotypes | Grade 4 invasive adenocarcinomas |

Ad-Cre

2.5x10^7 PFU (10 weeks)

AAV-Cre

0.1x10^9 VG (16 weeks)

0.5x10^9 VG (12 weeks)

2.5x10^9 VG (12 weeks)

12.5x10^9 VG (12 weeks)

◄**Fig. 2** Substituting the adeno-Cre with an AAV-Cre virus results in a similar onset and tumor stage pattern of the disease as observed in the original KP model. **A** Hematoxylin & Eosin (H&E)-stained lung tissue sections after transduction with adeno-Cre and various AAV-Cre titers. Scale bar = 5000 μm. **B** Higher magnification of H&E-stained lung sections featuring different stages of tumor development. Column 1: lesions of grade 1 atypical adenomatous hyperplasia (AAH) progressing to small adenoma, column 2: grade 2 adenomas, column 3: grade 2 adenomas featuring uniform nuclei, column 4: grade 3 adenocarcinomas featuring pleomorphic nuclei, column 5: grade 3 adenocarcinomas displaying mixed cellular phenotypes, and column 6: grade 4 invasive adenocarcinomas

cobalt and zinc resulted in a more than 30-fold increased transduction efficiency of AAV2 vectors [37]. From a pragmatic perspective, although modifications to the transduction protocol could reduce costs by decreasing the amount of viral solution required, the adapted protocol would need to be re-titrated to achieve the desired number of tumors.

Previously, it has been shown that total tumor and vascular volume increase over time in a dose-dependent manner in the KP lung cancer model [19]. Specifically, it was reported that during a 12-week period, beginning at week 8, total tumor and vascular volume increased approximately twofold and fivefold, respectively, following induction with a low and a high AV-Cre vector titer. Consistent with this, normalized lung volume was also reduced approximately fourfold over an eight-week period beginning at week 4 following induction with a high AAV-Cre vector titer. Thus, the AV- and AAV-based vectors resulted in comparable disease progression, but further experiments would be required to determine the relative proportion of each stage at different time points in the two models. Based on the analysis of lung H&E sections, quantifying the total number of tumor nodules per animal was challenging since the tumor stage of the individual nodules was very heterogeneous. In detail, determining the individual tumor stage of the single nodules requires the expertise of a trained pathologist. Thus, our study reported a qualitative analysis of the tumor stage, which showed that substituting the lentiviral vector with the AAV-Cre vector did not result in a dramatic change in the tumor stage distribution. The exact tumor number per vector dose was not reported in the original lung KP protocol, which concluded that tumor numbers and time to progression of autochthonous mouse tumor models vary widely depending on the strain/background of the mice as well as other factors that vary from institution to institution [12]. Thus, it would be interesting in future studies to compare the detailed disease status and progression induced by the AV- and AAV-based systems and to determine the exact tumor-inducing capacity of the novel AAV-Cre vector in extreme limiting dilution assays.

In a study aimed at comparing the effect of different treatment regimens on tumor growth, the number of animals required for statistically significant results can be reduced by minimizing differences in tumor burden between animals at the start of treatment. We observed significant differences in tumor burden between animals 8 weeks after the instillation with a high virus titer (Fig. S1). Thus, micro-CT-guided individualization of the time point of treatment initiation would allow for a reduction in differences not only in disease burden but also in the associated tumor stage, which changes during disease progression.

In tumor models, the use of humane endpoints allows for early termination of experiments and minimizes animal discomfort, suffering, and pain while ensuring that scientific goals are met [36]. Based on previously published protocols [11, 19, 48], our study provides an open-source protocol for analyzing micro-CT data to monitor tumor growth over time by quantifying "net change in lung volume." The drop in lung volume over time preceded the loss of body weight (Fig. 3B), which is also considered a humane endpoint [36]. Ideally, to determine whether our micro-CT protocol is appropriate for measuring tumor growth over time, a benchmark comparison with other methods should be performed, such as determining tumor growth by immunohistochemistry at various endpoints. Nevertheless, the quantification of "net change in lung volume" might be well suited for the early identification of animals harboring a high tumor load and thus are at a higher risk of suffering or death thereby clearly contributing to compliance with the 3Rs principles.

A shortcoming of our study is that we did not benchmark our CT-based protocol to determine tumor growth over time. Further, we did not explicitly test whether Cre is still expressed in the induced tumors. In detail, it has been shown that the constitutive endonuclease activity of Cre significantly reduces the proliferation of mammalian cells [32] and that the inducible expression of Cre induced regression of primary lymphomas in p53-deficient mice [31]. However, gutless AAV vectors are unable to integrate and their cargo DNA is lost over time as their transgenes exist in the host cell nucleus as non-replicating episomes [9, 20]. However, in the context of using the KP model to study immunotherapy [16], it would be of interest to observe in subsequent studies how Cre is expressed in the KP model over time. In addition, a variety of serotypes are available for AAV-based vectors, which could serve as unique tools to further study tumorigenesis and lung cancer development in the KP model [34] in the absence of the immune response induced by the adeno-Cre-based system [38]. In the context of the immune response, further studies will be necessary to examine whether the AAV-based vectors also infect immune cells, particularly macrophages resident in the lung microenvironment as it was shown previously for adeno-Cre-based viruses [40]. Finally, it would be interesting to characterize in detail how the serotype and capsid choice affect the cellular tropism of AAV-based vectors and consequently the tumor-associated immune response.
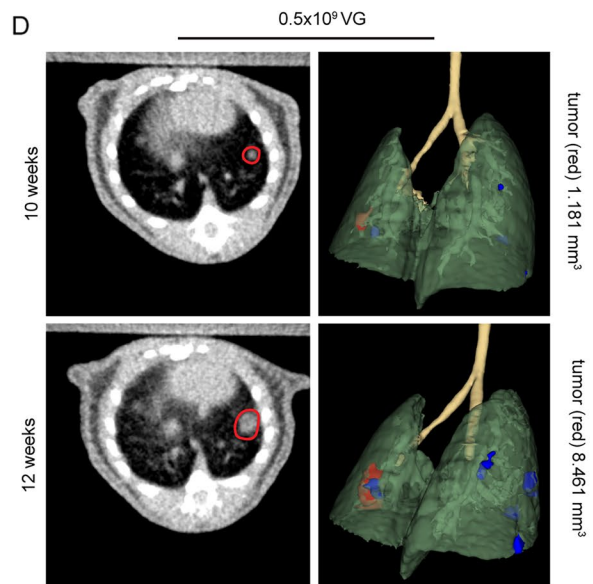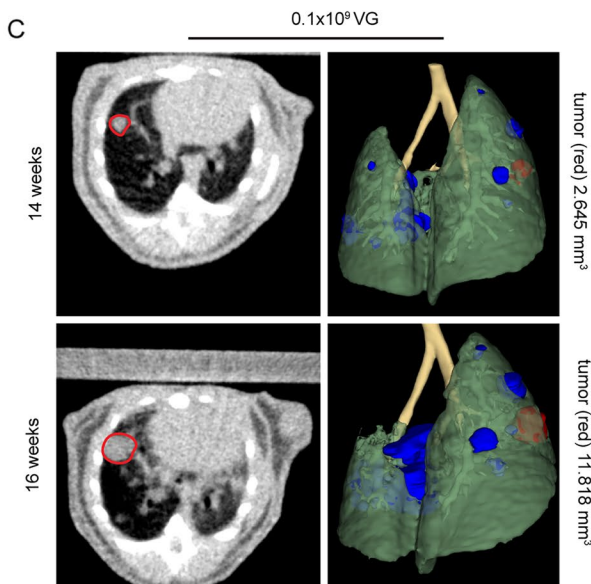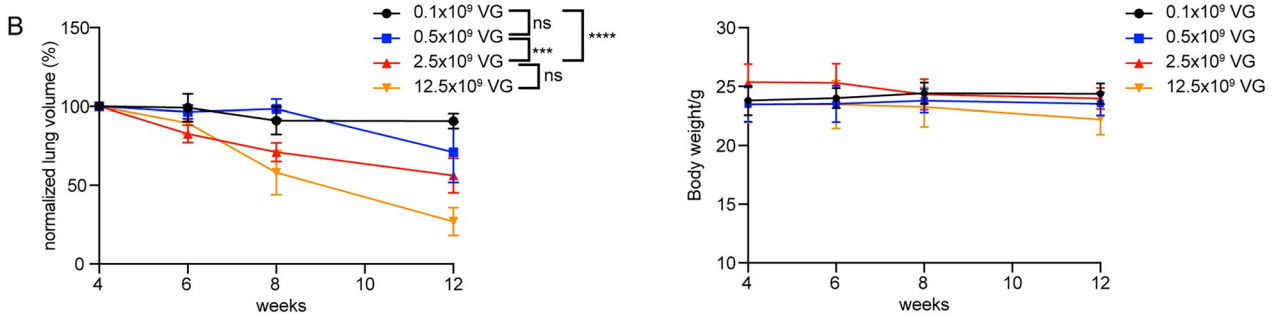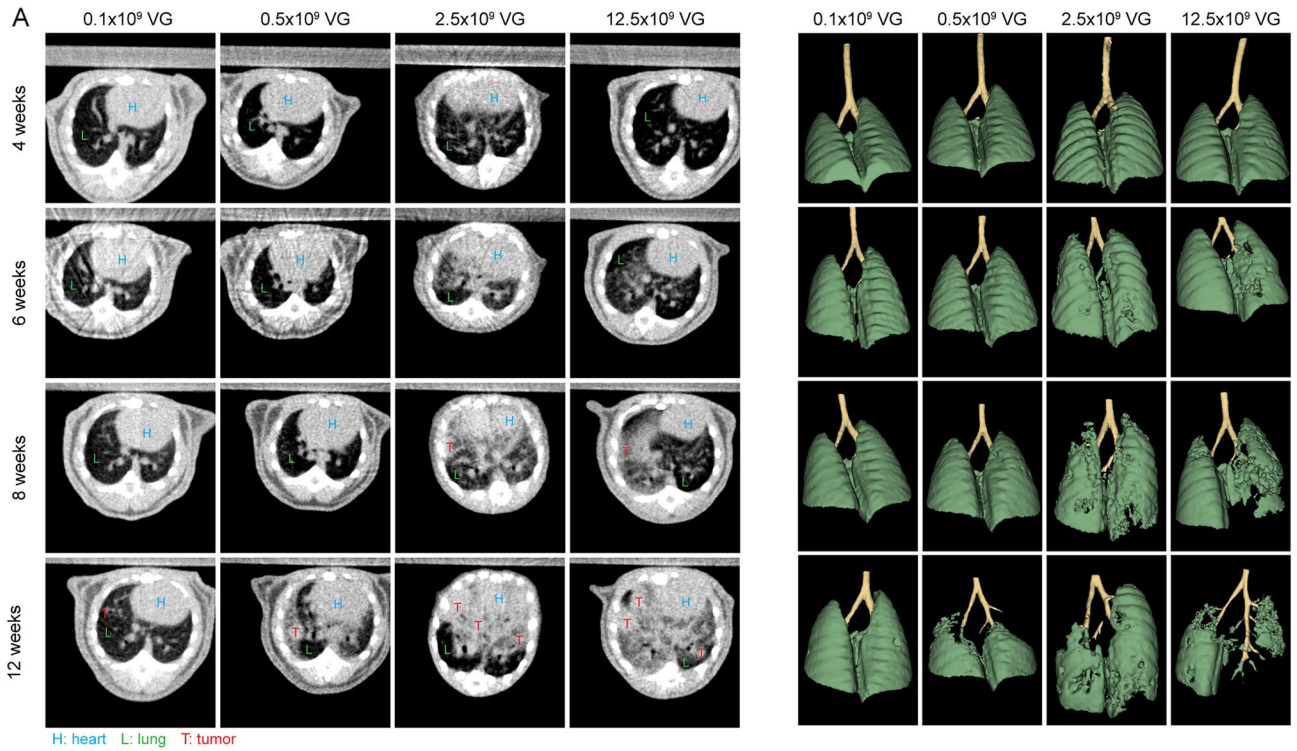
H: heart   L: lung   T: tumor

◄**Fig. 3** Longitudinal monitoring of tumor growth by micro-CT and 3D reconstruction. **A** Tumor growth was monitored longitudinally by micro-CT after inoculation with the indicated vector titers. The heart (H), lungs (L), and tumors (T) are directly identified on the images by respective labels. (left side). 3D reconstruction of functional lung volume was calculated using the 3D Slicer software (right side). **B** Quantification of normalized lung volume over time of animals after inoculation with the indicated vector titers. Data are presented as mean $\pm$ SEM, $n = 3$–4 mice. Two-way ANOVA, multiple comparisons, *ns* no significant difference, ***$P < 0.001$, ****$P < 0.0001$. **C** After inoculation with a low vector titer of 0.1×10^9 VG, individual nodules were identifiable by micro-CT and could be followed over time (see red marked nodules). **D** Similar results were obtained after inoculation with a vector titer of 0.5×10^9 VG

Conclusions

In summary, by substituting the adenoviral/lenti-Cre vector with an AAV-Cre vector, our adapted protocol allows handling the KP mouse model under BSL-1 conditions so that virus-transduced animals can be repeatedly analyzed by micro-CT, thereby drastically reducing the number of animals required for longitudinal monitoring of tumor growth. Also, in compliance with the 3R principle, optimizing the anesthesia protocol and switching to microscope-guided viral instillation increases productivity and reduces procedure-related complications. Finally, our user-friendly protocol for 3D reconstruction of tumor volume using open-source software will further foster the broad applicability of the KP tumor model.

Methods

Intratracheal delivery of a viral vector encoding Cre recombinase into the Kras-Lox-STOP-Lox-G12D p53 flox/flox (KP) mouse model faithfully recapitulates human lung adenocarcinoma. Handling virus-based delivery systems requires elevated biosafety measures, e.g., a biosafety level 2 (BSL-2) infrastructure. However, in animal research facilities, small animal micro-computed tomography (micro-CT) equipment is typically stored in general access areas, e.g., in BSL-1 compartments. Our goal was to adapt the protocol so that the Cre-induced KP mouse model could be handled during the entire procedure under BSL-1 conditions, allowing repeated micro-CT analyses of individual animals, thereby dramatically reducing the number of animals required for longitudinal monitoring of tumor growth.

Mouse model

The Kras$^{LSL-G12D/+}$;Trp53$^{fl/fl}$ mice were bred and obtained from our in-house animal facility at the University of Bern, Switzerland. In detail, Kras$^{LSL-G12D/+}$;Trp53$^{fl/fl}$ mice were generated by crossing stock B6.129SS4-krastm4Tyj/J

mice with B6.129P2-Trp53tm1Brn/J [25, 33]. All animal experiments were carried out in accordance with protocols approved by the local ethics committee of the Canton of Bern; license number PB_2016-01560 and BE49_2022.

Anesthesia

The mouse experiments were performed in accordance with the animal welfare guidelines and protocols approved by the institutional animal care and ethical committee, i.e., the ethic commission of the Canton of Bern, Switzerland, license number BE49_2022. The protocol was developed based on a publication by Henke and Erhardt [15], whereas the composition of the fully reversible anesthesia was based on a publication by Henke and Müller [21]. In detail, mice at 8 weeks of age were anesthetized with a solution containing 30% Ketalar (Pfizer, Cat. No. 35073), 20% Domitor (Orion, Cat. No. 50590), and 12.7% fentanyl (Mepha, cat. no. 53987) in 0.9% Sodium chloride (NaCl, B. Braun, Cat. No. 3570130) by intraperitoneal (i.p.) injection [1]. After vector instillation, mice were immediately administered an antagonist solution containing 10% Revertor (Virbac, Cat. No. 58701) and 60% Naloxone (Mepha, Cat. No. 56952) in 0.9% NaCl by i.p. injection. This anesthetic protocol avoids unnecessary stress to the animal and allows very regular breathing throughout the procedure, allowing smooth intubation of the animals without accidental ingestion of the virus suspension. Further details are given in the 'Step-by-step procedure' section.

Vector information and preparation of virus-containing solutions

AAV2/9-cmv-Cre: the genome is flanked by the inverted terminal repeats of AAV serotype 2 and is packaged in the capsid of AAV serotype 9. Transcription of recombinant Cre recombinase is driven by a cytomegalovirus (CMV) promoter. AAV2/9-cmv-Cre was produced by the Bertarelli Foundation Gene Therapy Platform at the Swiss Federal Institute of Technology, Lausanne (https://www.epfl.ch/research/facilities/gene-therapy/. The platform can customize any construct with one or more sequences of interest and/or perform complete design and cloning of the transfer construct. A wide range of vector backbones (AAVs and lentiviruses) are available, including a variety of promoters, reporter genes, and enhancers). Specifically, the high titer and high purity AAV vector batches were generated by transient transfection with a two-plasmid system of mammalian cells (HEK293) grown in orbitally shaken suspension cultures as previously described [7]. The original vector was freshly diluted with Minimal Essential Media (MEM, Sigma-Aldrich, cat. no. M8042) to various titers. Then,

Fig. 4 Individually forming tumor nodules are differentially infiltrated by CD8-positive cells after inoculation with a low vector titer. Imaging mass cytometry visualization of two tumor nodules from the same animal 10 weeks after vector instillation. **A** Imaging mass cytometry visualization of E-cadherin (green), CD8 (white), and DNA (blue). **B** Same analysis of a different lesion from the same animal
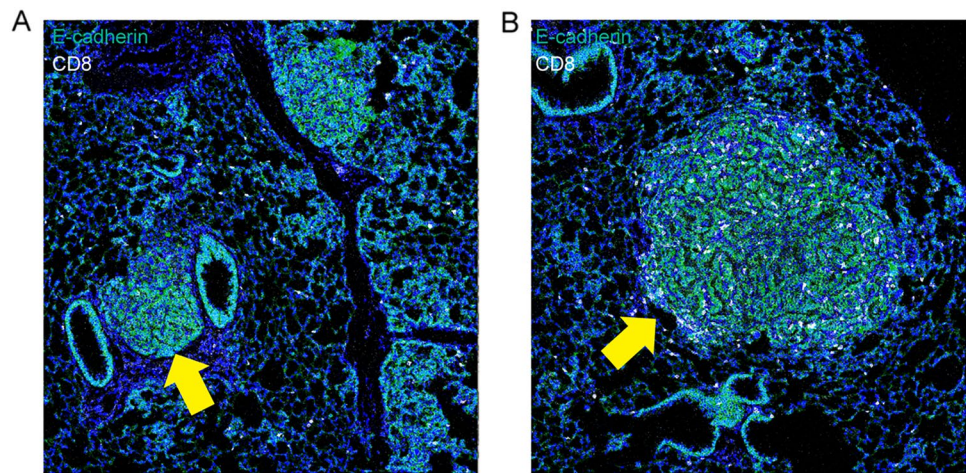
CaCl$_2$ was added to a final concentration of 10 mM, and the solutions were incubated for 20 min at room temperature.

Ad5CMVCre: adenoviral vector with CMV (Cytomegalovirus) promoter driving the expression of the Cre Recombinase protein (https://vector-core.medicine.uiowa.edu/products/ad5cmvcre?variant=40576502096). Ad5CMVCre was purchased from the University of Iowa, Gene Transfer Vector Core.

Preparation and administration of virus-containing solutions should occur in a biosafety hood and follow all guidelines for BSL-2 research.

Vector administration

Solutions containing vectors at various concentrations were administered to animals by intratracheal instillation monitored through a stereomicroscope (Nikon SMZ645, zoom range of 0.8×–5× magnification). The technical details are described in the "Step-by-step procedure" section. See also the supplementary video of the publication of DuPage et al. [12].

micro-CT scan and image analysis

Beginning 2 weeks after vector instillation, lungs were examined weekly using an X-RAD SmART Precision X-Ray Imaging System (Precision X-Ray, North Branford, CT) to confirm tumor formation. In detail, mice were continuously anesthetized with 3% isoflurane. Photons were filtered using a 2 mm Al filter for computed tomography. The raw DICOM data were imported into the 3D slicer for visualization and quantitative analysis [42]. For lung volume analysis, automatic segmentation of the lungs and airways was performed based on the "Grow from Seeds" tool. Subsequently, the "Segment Statistics" tool was used to quantify lung volume. For tumor volume analysis, the window and level in "Volumes" were adjusted to better separate lung and tumor.

Subsequently, tumors were segmented in "Segmentation Editor" and quantified using "Segment statistics." After segmentation, 3D reconstruction was performed.

Immunohistochemistry

Hematoxylin & Eosin (H&E) staining was performed as previously described [5].

Imaging mass cytometry

Imaging mass cytometry (IMC) was performed using an optimized mouse antibody panel for FFPE tissues [6] In brief, 3 μm sections of FFPE mouse lung tissues were sectioned and dried overnight. Antigen retrieval, blocking and staining with metal-labeled antibodies were performed the following day (use same reference as above). On day three, DNA was stained with intercalator-Ir (iridium) and the sections were acquired on the Hyperion tissue imager (Standard BioTools) at the University of Bern/Inselspital IMC platform (www.imc.unibe.ch). The mass cytometry data (MCD) file was loaded into napari: multi-dimensional image viewer for python (Sofroniew [39]) and the napari-imc plugin was downloaded and employed [47]. We visualized the channels for DNA in blue, E-cadherin (tumor) in green, and CD8 (cytotoxic T cells) in white (Fig. 4).

Statistical analysis

Statistical analysis was performed using GraphPad Prism 9. Results were collected from at least three different mice. Error bars represent the mean ± standard error of the mean (SEM). Two-way ANOVA was performed as described in the figure legends. The p values < 0.05 were considered significant. In all analyses, the significance level is indicated as follows: *$P < 0.05$, **$P < 0.01$, ***$P < 0.001$, ****$P < 0.0001$.

Step-by-step procedures

Necessary equipment

1 mL syringes and needles	Hanging tray
Pipette P100	Rubber air blower
Pipette P10	Forceps
Pipette tips	Lamp
Cannula 20 G and 18 G	Microscope (0.8×–5× magnification)
Heating pad	

Prepare anesthesia as a batch solution ($n + 1$), and keep it at room temperature. Prepare 100 µl per animal:

Anesthesia solution

- 300 µl Ketalar 50 mg/ml
- 200 µl Domitor 1 mg/ml
- 127 µl Fentanyl 0.05 mg/ml
- 373 µl NaCl·0.9%

Antagonist solution

- 100 µl Revertor 5 mg/ml
- 600 µl Naloxone 0.4 mg/ml
- 300 µl NaCl 0.9%

Virus solution

- Virus solution x µl virus + y µl MEM + 2.5 µl $CaCl_2$·0.2 M
- Total volume 50 µl

Prepare the virus solution in a total volume of 50 µl per animal, and adjust the concentration accordingly (Record details in the lab book).

Anesthesia (timing: 10 min per cage of 5 mice)

1. Anesthetize the animal by intraperitoneal (i.p.) injection of 80 µl of the prepared anesthetic solution (regardless of differences in body weight).
2. Confirm that the mice are fully anesthetized by ensuring they lack a toe reflex.
3. If not, inject another 20 µl of the anesthetic solution, i.p.
4. Place the animal on its stomach on the heating pad.

5. Apply Bepanthen eye ointment to both eyes.

Virus/Vector delivery by intratracheal instillation (Timing: 2–5 min per mouse)

6. Carefully position the animal by the upper teeth in the hanging rack (Fig. 1A).
7. Place the lamp directly on the neck of the animal (Fig. 1A).
8. Fix the tail of the animal with a small piece of adhesive tape.
9. Open the mouth gently with a small forceps using the right hand.
10. Use a second forceps equipped with rubber end caps to gently pull out the tongue with the left hand to the left side (Fig. 1B).
11. Use the stereomicroscope to identify the trachea (pulsating in the center) (Fig. 1C).
12. To fully open the mouth, adjust the tail's position by moving the adhesive tape (Fig. 1C).
13. Fully open the trachea by slightly adjusting the forceps.
14. Insert the cannula (attached to the catheter) into the trachea (Fig. 1D). There should be no resistance while inserting the catheter into the trachea.
15. Remove the cannula from the catheter.
16. Place a rubber air blower on the catheter, administer an air bolus, and check if the lungs expand. If the lungs are not expanding, the catheter might be in the esophagus. In this case, gently remove the catheter and repeat the two previous steps. Repeat until the lungs expand visually after applying a bolus of air (Fig. 1E).
17. Pipette the virus solution directly into the opening of the catheter to ensure the entire volume is inhaled (Fig. 1F).
18. When the catheter is correctly inserted into the trachea, the mouse immediately begins to inhale the solution. Once the solution is no longer visible in the opening of the catheter, wait a few seconds for all of the solution to run down the catheter.
19. Add an air bolus with a rubber air blower.
20. Remove the catheter from the trachea.
21. Immediately remove the animal from the hanging rack.
22. Place the mouse on its side on the heat pad.
23. Open its mouth with forceps to facilitate breathing.

Animal recovery (Timing: 10 min recovery time)

24. Inject 0.1 ml of the antagonist solution i.p. (do not delay this step).
25. Leave the mouse on the warming pad until fully awakened.
26. Put the mouse back in the cage.

27. Monitor the animal until breathing becomes steady again.
28. Add the "omnivore" sign if necessary.
29. Place the cage back in the animal room.
30. Check the animal the next day (or in the afternoon if anesthesia was performed in the morning).

Author contributions HD, PD and TMM conceived the project, designed the experiments and wrote the manuscript. HD, HG and CD performed most experiments, analyzed the data and prepared the figures. TL collected and analyzed patient samples and participated in writing the corresponding methods and results section. MM, GK, SMM and FEB helped to establish the animal model. TMB and DS performed the IMC image acquisition and analysis and wrote the corresponding methods and results. WW, RP HD, PD and TMM edited the manuscript. All authors read and approved the final manuscript. PD and TMM contributed equally to this study.

Availability of data and material All data generated or analyzed during this study are included in this published article and its supplementary information files.

Declarations

Conflict of interest The authors declare no conflict of interest.

Ethical approval As described above, all animal experiments were carried out in accordance with protocols approved by the local ethics committee of the Canton of Bern; license number PB_2016-01560BE49_2022, national number 34192.

Consent for publication Not applicable.

References

1. Ahmadi-Noorbakhsh S, Abbasi MF, Ghasemi M, Bayat G, Davoodian N, Sharif-Paghaleh E, Poormoosavi SM, Rafizadeh M, Maleki M, Shirzad-Aski H, Jahromi HK, Dadkhah M, Khalvati B, Safari T, Behmanesh MA, Khoshnam SE, Houshmand G, Talaei SA (2022) Anesthesia and analgesia for common research models of adult mice. Lab Anim Res 38:40
2. Albrecht M, Henke J, Tacke S, Markert M, Guth B (2014) Effects of isoflurane, ketamine-xylazine and a combination of medetomidine, midazolam and fentanyl on physiological variables continuously measured by telemetry in Wistar rats. BMC Vet Res 10:198
3. Annoni A, Gregori S, Naldini L, Cantore A (2019) Modulation of immune responses in lentiviral vector-mediated gene transfer. Cell Immunol 342:103802
4. Atasheva S, Yao J, Shayakhmetov DM (2019) Innate immunity to adenovirus: lessons from mice. FEBS Lett 593:3461–3483
5. Berezowska S, Galvan JA (2017) Immunohistochemical detection of the autophagy markers LC3 and p62/SQSTM1 in formalin-fixed and paraffin-embedded tissue. Methods Mol Biol 1560:189–194
6. Birrer F, Brodie T, Stroka D (2023) OMIP-088: twenty-target imaging mass cytometry panel for major cell populations in mouse formalin fixed paraffin embedded liver. Cytometry A 103:189–192
7. Blessing D, Vachey G, Pythoud C, Rey M, Padrun V, Wurm FM, Schneider BL, Déglon N (2019) Scalable production of AAV vectors in orbitally shaken HEK293 cells. Mol Ther-Methods Clin Dev 13:14–26
8. Buitrago S, Martin TE, Tetens-Woodring J, Belicha-Villanueva A, Wilding GE (2008) Safety and efficacy of various combinations of injectable anesthetics in BALB/c mice. J Am Assoc Lab Anim Sci 47:11–17
9. Chandler RJ, Sands MS, Venditti CP (2017) recombinant adeno-associated viral integration and genotoxicity: insights from animal models. Hum Gene Ther 28:314–322
10. Collins DE, Reuter JD, Rush HG, Villano JS (2017) Viral vector biosafety in laboratory animal research. Comp Med 67:215–221
11. Deng H, Gao Y, Trappetti V, Hertig D, Karatkevich D, Losmanova T, Urzi C, Ge H, Geest GA, Bruggmann R, Djonov V, Nuoffer J-M, Vermathen P, Zamboni N, Riether C, Ochsenbein A, Peng R-W, Kocher GJ, Schmid RA, Dorn P, Marti TM (2022) Targeting lactate dehydrogenase B-dependent mitochondrial metabolism affects tumor initiating cells and inhibits tumorigenesis of non-small cell lung cancer by inducing mtDNA damage. Cell Mol Life Sci 79(8):445
12. DuPage M, Dooley AL, Jacks T (2009) Conditional mouse lung cancer models using adenoviral or lentiviral delivery of Cre recombinase. Nat Protoc 4:1064–1072
13. Dupage M, Cheung AF, Mazumdar C, Winslow MM, Bronson R, Schmidt LM, Crowley D, Chen J, Jacks T (2011) endogenous t cell responses to antigens expressed in lung adenocarcinomas delay malignant tumor progression. Cancer Cell 19:72–85

14. Dupage M, Mazumdar C, Schmidt LM, Cheung AF, Jacks T (2012) Expression of tumour-specific antigens underlies cancer immunoediting. Nature 482:405–409

15. Erhardt W, Henke J, Lendl C (2002) Narkose-Notfälle. Haug Fachbuchverlag, Karl F

16. Fitzgerald B, Connolly KA, Cui C, Fagerberg E, Mariuzza DL, Hornick NI, Foster GG, William I, Cheung JF, Joshi NS (2021) A mouse model for the study of anti-tumor T cell responses in Kras-driven lung adenocarcinoma. Cell Rep Methods 1(5):100080

17. Foster WK, Ford NL (2011) Investigating the effect of longitudinal micro-CT imaging on tumour growth in mice. Phys Med Biol 56:315–326

18. Gallaher SD, Berk AJ (2013) A rapid Q-PCR titration protocol for adenovirus and helper-dependent adenovirus vectors that produces biologically relevant results. J Virol Methods 192:28–38

19. Haines BB, Bettano KA, Chenard M, Sevilla RS, Ware C, Angagaw MH, Winkelmann CT, Tong C, Reilly JF, Sur C, Zhang W (2009) A quantitative volumetric micro-computed tomography method to analyze lung tumors in genetically engineered mouse models. Neoplasia 11:39–47

20. Harno E, Ec C, White A (2013) Metabolic pitfalls of CNS Cre-based technology. Cell Metab 18:21–28

21. Henke J, Müller D (2017) Vollstandig antagonisierbare lnjektionsnarkose bei Kleinsaugern (Nager, Meerschweinchen, Kaninchen). www.docplayer.org. online: docplayer

22. Herbst RS, Heymach JV, Lippman SM (2008) Lung cancer. N Engl J Med 359:1367–1380

23. Herter-Sprie GS, Korideck H, Christensen CL, Herter JM, Rhee K, Berbeco RI, Bennett DG, Akbay EA, Kozono D, Mak RH, Mike Makrigiorgos G, Kimmelman AC, Wong K-K (2014) Image-guided radiotherapy platform using single nodule conditional lung cancer mouse models. Nat Commun 5:5870

24. Jackson EL, Olive KP, Tuveson DA, Bronson R, Crowley D, Brown M, Jacks T (2005) The differential effects of mutant p53 alleles on advanced murine lung cancer. Cancer Res 65:10280–10288

25. Jackson EL, Willis N, Mercer K, Bronson RT, Crowley D, Montoya R, Jacks T, Tuveson DA (2001) Analysis of lung tumor initiation and progression using conditional expression of oncogenic K-ras. Genes Dev 15:3243–3248

26. Jaynes JM, Sable R, Ronzetti M, Bautista W, Knotts Z, Abisoye-Ogunniyan A, Li D, Calvo R, Dashnyam M, Singh A, Guerin T, White J, Ravichandran S, Kumar P, Talsania K, Chen V, Ghebremedhin A, Karanam B, Bin Salam A, Amin R, Odzorig T, Aiken T, Nguyen V, Bian Y, Zarif JC, de Groot AE, Mehta M, Fan L, Hu X, Simeonov A, Pate N, Abu-Asab M, Ferrer M, Southall N, Ock CY, Zhao Y, Lopez H, Kozlov S, de Val N, Yates CC, Baljinnyam B, Marugan J, Rudloff U (2020) Mannose receptor (CD206) activation in tumor-associated macrophages enhances adaptive and innate antitumor immune responses. Sci Transl Med 12(530):eaax6337

27. Kersten K, Visser KE, Miltenburg MH, Jonkers J (2017) Genetically engineered mouse models in oncology research and cancer medicine. EMBO Mol Med 9:137–153

28. Kim H, Kim M, Im SK, Fang S (2018) Mouse Cre-LoxP system: general principles to determine tissue-specific roles of target genes. Lab Anim Res 34:147–159

29. Kirsch DG, Dinulescu DM, Miller JB, Grimm J, Santiago PM, Young NP, Nielsen GP, Quade BJ, Chaber CJ, Schultz CP, Takeuchi O, Bronson RT, Crowley D, Korsmeyer SJ, Yoon SS, Hornicek FJ, Weissleder R, Jacks T (2007) A spatially and temporally restricted mouse model of soft tissue sarcoma. Nat Med 13:992–997

30. Kirsch DG, Grimm J, Guimaraes AR, Wojtkiewicz GR, Perez BA, Santiago PM, Anthony NK, Forbes T, Doppke K, Weissleder R, Jacks T (2010) Imaging primary lung cancers in mice to study radiation biology. Int J Radiat Oncol Biol Phys 76:973–977

31. Li Y, Choi PS, Casey SC, Felsher DW (2014) Activation of Cre recombinase alone can induce complete tumor regression. PLoS ONE 9:e107589

32. Loonstra A, Marc Vooijs H, Beverloo B, Allak BA, Van Drunen E, Kanaar R, Berns A, Jonkers J (2001) Growth inhibition and DNA damage induced by Cre recombinase in mammalian cells. Proc Natl Acad Sci 98:9209–9214

33. Marino S, Vooijs M, van der Gulden H, Jonkers J, Berns A (2000) Induction of medulloblastomas in p53-null mutant mice by somatic inactivation of Rb in the external granular layer cells of the cerebellum. Genes Dev 14:994–1004

34. Marjanovic ND, Hofree M, Chan JE, Canner D, Katherine Wu, Trakala M, Hartmann GG, Smith OC, Kim JY, Evans KV, Hudson A, Ashenberg O, Porter CBM, Bejnood A, Subramanian A, Pitter K, Yan Y, Delorey T, Phillips DR, Shah N, Chaudhary O, Tsankov A, Hollmann T, Rekhtman N, Massion PP, Poirier JT, Mazutis L, Li R, Lee J-H, Amon A, Rudin CM, Jacks T, Regev A, Tammela T (2020) Emergence of a high-plasticity cell state during lung cancer evolution. Cancer Cell 38:229–246

35. Mayers JR, Wu C, Clish CB, Kraft P, Torrence ME, Fiske BP, Yuan C, Bao Y, Townsend MK, Tworoger SS, Davidson SM, Papagiannakopoulos T, Yang A, Dayton TL, Ogino S, Stampfer MJ, Giovannucci EL, Qian ZR, Rubinson DA, Ma J, Sesso HD, Gaziano JM, Cochrane BB, Liu S, Wactawski-Wende J, Manson JE, Pollak MN, Kimmelman AC, Souza A, Pierce K, Wang TJ, Gerszten RE, Fuchs CS, Vander Heiden MG, Wolpin BM (2014) Elevation of circulating branched-chain amino acids is an early event in human pancreatic adenocarcinoma development. Nat Med 20:1193–1198

36. Jie M (2019) Refining humane endpoints in mouse models of disease by systematic review and machine learning-based endpoint definition. Altex 36(4):555–571

37. Rambhai HK, Ashby FJ, Qing K, Srivastava A (2020) Role of essential metal ions in AAV vector-mediated transduction. Mol Ther-Methods Clin Dev 18:159–166

38. Shirley JL, de Jong YP, Terhorst C, Herzog RW (2020) Immune responses to viral gene therapy vectors. Mol Ther 28:709–722

39. Ahlers, J., Althviz, D., Amsalem, O., Anderson, A., Bokota, G., Boone, P., Bragantini, J., Buckley, K., Burt, A., Bussonnier, M., Can Solak, A., Caporal, C., Doncila Pop, D., Evans, K., Gaifas, L., Freeman, J., Gohlke, C., Gunalan, K., Har-Gil, H., Harfouche, M., Harrington, K., Hilsenstein, V., Hutchings, K., Lambert, T., Lauer, J., Lichtner, G., Liu, Z., Liu, L., Marconato, L. & Martin, S. et al. Napari: a multi-dimensional image viewer for python, Zenodo, https://doi.org/10.5281/zenodo.8115575 (2023).

40. Tippimanchai DD, Nolan K, Poczobutt J, Verzosa G, Li H, Scarborough H, Huang J, Young C, DeGregori J, Nemenoff RA, Malkoski SP (2018) Adenoviral vectors transduce alveolar macrophages in lung cancer models. OncoImmunology 7:e1438105

41. Der Loo V, Johannes CM, Fraser Wright J (2016) Progress and challenges in viral vector manufacturing. Hum Mol Genet 25:R42–R52

42. Velazquez ER, Parmar C, Jermoumi M, Mak RH, Van Baardwijk A, Fennessy FM, Lewis JH, De Ruysscher D, Kikinis R, Lambin P, Aerts HJ (2013) Volumetric CT-based segmentation of NSCLC using 3D-Slicer. Sci Rep 3(1):3529

43. Verdera HC, Kuranda K, Mingozzi F (2020) AAV vector immunogenicity in humans: a long journey to successful gene transfer. Mol Ther 28:723–746

44. Walters RW, Duan D, Engelhardt JF, Welsh MJ (2000) Incorporation of adeno-associated virus in a calcium phosphate coprecipitate improves gene transfer to airway epithelia in vitro and in vivo. J Virol 74:535–540

45. Wang D, Tai PWL, Gao G (2019) Adeno-associated virus vector as a platform for gene therapy delivery. Nat Rev Drug Discovery 18:358–378

46. Westcott PMK, Sacks NJ, Schenkel JM, Ely ZA, Smith O, Hauck H, Jaeger AM, Zhang D, Backlund CM, Beytagh MC, Patten JJ, Elbashir R, Eng G, Irvine DJ, Yilmaz OH, Jacks T (2021) Low neoantigen expression and poor T-cell priming underlie early immune escape in colorectal cancer. Nat Cancer 2:1071–1085

47. Windhager J, Bodenmiller B, Eling N (2021) An end-to-end workflow for multiplexed image processing and analysis. In: bioRxiv

48. Xie H, Hanai J, Ren JG, Kats L, Burgess K, Bhargava P, Signoretti S, Billiard J, Duffy KJ, Grant A, Wang X, Lorkiewicz PK, Schatzman S, Bousamra M 2nd, Lane AN, Higashi RM, Fan TW, Pandolfi PP, Sukhatme VP, Seth P (2014) Targeting lactate dehydrogenase–a inhibits tumorigenesis and tumor progression in mouse models of lung cancer and impacts tumor-initiating cells. Cell Metab 19:795–809

49. Yang H, Liang SQ, Schmid RA, Peng RW (2019) New horizons in KRAS-mutant lung cancer: dawn after darkness. Front Oncol 9:953

Authors and Affiliations

Haibin Deng[1,2,9,10] · Huixiang Ge[1,2,3] · Christelle Dubey[1,2] · Tereza Losmanova[4] · Michaela Medová[2,5] · Georgia Konstantinidou[6] · Seyran Mathilde Mutlu[2,7] · Fabienne Esther Birrer[8,2] · Tess Melinda Brodie[8,2] · Deborah Stroka[8,2] · Wenxiang Wang[9,10] · Ren-Wang Peng[1,2] · Patrick Dorn[1,2] · Thomas Michael Marti[1,2]

✉ Ren-Wang Peng
renwang.peng@insel.ch

✉ Patrick Dorn
patrick.dorn@insel.ch

✉ Thomas Michael Marti
thomas.marti@insel.ch

1. Department of General Thoracic Surgery, Inselspital, Bern University Hospital, University of Bern, Murtenstrasse 28, 3008 Bern, Switzerland

2. Department for BioMedical Research, University of Bern, Bern, Switzerland

3. Graduate School of Cellular and Biomedical Sciences, University of Bern, Bern, Switzerland

4. Institute of Pathology, University of Bern, Bern, Switzerland

5. Department of Radiation Oncology, Inselspital, Bern University Hospital, University of Bern, Bern, Switzerland

6. Institute of Pharmacology, University of Bern, Bern, Switzerland

7. Department of Pulmonary Medicine, Inselspital, Bern University Hospital, University of Bern, Bern, Switzerland

8. Department of Visceral Surgery and Medicine, Inselspital, Bern University Hospital, University of Bern, Bern, Switzerland

9. Thoracic Surgery Department 2, Hunan Cancer Hospital and the Affiliated Cancer Hospital of Xiangya School of Medicine, Central South University, Changsha 410013, Hunan, China

10. Hunan Key Laboratory of Translational Radiation Oncology, Hunan Cancer Hospital and the Affiliated Cancer Hospital of Xiangya School of Medicine, Central South University, Changsha 410013, China